AGU PUBLICATIONS

JGR

Journal of Geophysical Research: Biogeosciences

RESEARCH ARTICLE
10.1002/2014JG002883

Key Points:
- Nitrate isotopes indicate microbial nitrate in high-centered polygons
- No clear primary isotopic signal of atmospheric nitrate in active layer soils
- Permafrost nitrate isotopes intermediate to microbial and atmospheric nitrate

Supporting Information:
- Supporting Information S1

Correspondence to:
J. M. Heikoop,
jheikoop@lanl.gov

Citation:
Heikoop, J. M., et al. (2015), Isotopic identification of soil and permafrost nitrate sources in an Arctic tundra ecosystem, *J. Geophys. Res. Biogeosci.*, *120*, 1000–1017, doi:10.1002/2014JG002883.

Received 8 DEC 2014
Accepted 6 MAY 2015
Accepted article online 13 MAY 2015
Published online 8 JUN 2015

Isotopic identification of soil and permafrost nitrate sources in an Arctic tundra ecosystem

Jeffrey M. Heikoop[1], Heather M. Throckmorton[1], Brent D. Newman[1], George B. Perkins[1], Colleen M. Iversen[2], Taniya Roy Chowdhury[3,4], Vladimir Romanovsky[5], David E. Graham[3], Richard J. Norby[2], Cathy J. Wilson[1], and Stan D. Wullschleger[2]

[1]Earth and Environmental Sciences Division, Los Alamos National Laboratory, Los Alamos, New Mexico, USA, [2]Environmental Sciences Division, Oak Ridge National Laboratory, Oak Ridge, Tennessee, USA, [3]Biosciences Division, Oak Ridge National Laboratory, Oak Ridge, Tennessee, USA, [4]Now at Biological Sciences Division, Pacific Northwest National Laboratory, Richland, Washington, USA, [5]Permafrost Laboratory University of Alaska Fairbanks, Fairbanks, Alaska, USA

Abstract The nitrate (NO_3^-) dual isotope approach was applied to snowmelt, tundra active layer pore waters, and underlying permafrost in Barrow, Alaska, USA, to distinguish between NO_3^- derived from atmospheric deposition versus that derived from microbial nitrification. Snowmelt had an atmospheric NO_3^- signal with $\delta^{15}N$ averaging -4.8 ± 1.0‰ (standard error of the mean) and $\delta^{18}O$ averaging 70.2 ± 1.7‰. In active layer pore waters, NO_3^- primarily occurred at concentrations suitable for isotopic analysis in the relatively dry and oxic centers of high-centered polygons. The average $\delta^{15}N$ and $\delta^{18}O$ of NO_3^- from high-centered polygons were 0.5 ± 1.1‰ and -4.1 ± 0.6‰, respectively. When compared to the $\delta^{15}N$ of reduced nitrogen (N) sources, and the $\delta^{18}O$ of soil pore waters, it was evident that NO_3^- in high-centered polygons was primarily from microbial nitrification. Permafrost NO_3^- had $\delta^{15}N$ ranging from approximately -6‰ to 10‰, similar to atmospheric and microbial NO_3^-, and highly variable $\delta^{18}O$ ranging from approximately -2‰ to 38‰. Permafrost ice wedges contained a significant atmospheric component of NO_3^-, while permafrost textural ice contained a greater proportion of microbially derived NO_3^-. Large-scale permafrost thaw in this environment would release NO_3^- with a $\delta^{18}O$ signature intermediate to that of atmospheric and microbial NO_3. Consequently, while atmospheric and microbial sources can be readily distinguished by the NO_3^- dual isotope technique in tundra environments, attribution of NO_3^- from thawing permafrost will not be straightforward. The NO_3^- isotopic signature, however, appears useful in identifying NO_3^- sources in extant permafrost ice.

1. Introduction

Permafrost thaw due to warming and resulting decomposition of preserved soil organic carbon (C) are important climate feedbacks from the Arctic terrestrial environment to the atmosphere [e.g., *Shaver et al.*, 1992; *Schuur et al.*, 2008; *Hinzman et al.*, 2013]. Tundra soil organic matter (SOM) decomposition releases nitrogen (N) to the soil [*Weintraub and Schimel*, 2005]. Release of N can fertilize and stimulate both plant growth and microbial decomposition in tundra soils, which are typically low in nutrient availability [e.g., *Neff et al.*, 2002; *Mack et al.*, 2004; *Weintraub and Schimel*, 2005; *Nowinski et al.*, 2008]. N dynamics, therefore, will be a key determinant in the timing and magnitude of tundra C fluxes in a warming climate due to strong linkages between C and N cycles [*Shaver et al.*, 1992; *Hobbie et al.*, 2002; *Weintraub and Schimel*, 2005; *Xu et al.*, 2011].

Shaver et al. [1992] presented a simplified N budget [after *Chapin et al.*, 1980] for coastal wet sedge tundra at Barrow, Alaska, USA, the location of the study presented herein. Their budget shows that the dissolved inorganic N (DIN) pool in Barrow soils is about four orders of magnitude smaller than the soil organic N (SON) pool, which has a slow turnover rate. N inputs and outputs are small relative to internal cycling of N through processes such as nitrification, plant uptake, and litter production. New N inputs are from atmospheric deposition, N_2 fixation, and lateral inputs from water or drifting snow [*Shaver et al.*, 1992]. Another potential N input is from thawing permafrost, both directly and indirectly through degradation of previously frozen SOM and subsequent N mineralization [cf. *Keuper et al.*, 2012]. Permafrost thaw may stimulate activity of permafrost microbes, which could then release considerable C and nutrients [see review in *Jansson and Tas*, 2014]. N can leave the system through leaching/lateral transport and denitrification, though lateral transport will occur primarily during the brief spring snowmelt period and denitrification rates are relatively slow [*Shaver et al.*, 1992].

Nitrate (NO_3^-) was chosen as a focus of this study because of its interesting spatial distribution in the study area. Due to the presence of continuous permafrost preventing adequate vertical drainage, much of the landscape is saturated and not conducive to nitrification or NO_3^- stability. Polygonal landforms greatly influence landscape microtopography and the saturation and redox states of active layer soils, with increased ice-wedge degradation leading to slightly elevated, oxic terrain [*Gersper et al*., 1980; *Lipson et al*., 2010; *Zona et al*., 2011; *Lipson et al*., 2012; *Lipson et al*., 2013]. The study site contains high-centered polygons with slightly elevated centers as well as low-centered polygons with slightly elevated rims (see section 2.1 for a full description of the study site, including polygonal terrain). Higher concentrations of oxyanions, including NO_3^- and sulfate, have been found in the rims of low-centered polygons and the elevated centers of high-centered polygons in the Barrow area [*Gersper et al*., 1980; *Newman et al*., 2015]. Changes in the abundance of NO_3^- in response to warmer and drier conditions in the future could have implications for plant community composition and feedbacks to the climate [see review in *Iversen et al*., 2015]. Primary sources of NO_3^- in Barrow tundra soils include wet and dry atmospheric deposition, decomposition of SOM and plant litter and subsequent ammonification and nitrification (herein termed microbial NO_3^-) [*Shaver et al*., 1992], and, possibly, thawing permafrost.

The use of C, hydrogen (H), and O isotopes to characterize hydrology, C cycling, and paleoclimate in permafrost landscapes is well established [*Lacelle and Vasil'chuk*, 2013]. The NO_3^- dual isotope approach, however, has received less attention in such settings, though significant work has been done in High Arctic glacial systems [*Ansari et al*., 2013; *Nowak and Hodson*, 2014], in streams draining coastal tundra [*Tye and Heaton*, 2007] and tundra disturbed by active layer detachments [*Louiseize et al*., 2014], and in streams draining watersheds that include alpine tundra [*Campbell et al*., 2002]. The dual isotope measurement of N and O isotopes in NO_3^- can be useful in distinguishing atmospheric versus microbial sources [e.g., *Amberger and Schmidt*, 1987; *Kendall*, 1998; *Curtis et al*., 2011; *Tye and Heaton*, 2007; *Ansari et al*., 2013; *Louiseize et al*., 2014]. For example, *Tye and Heaton* [2007] were able to use this approach to demonstrate that snowpack NO_3^- was nearly completely assimilated by soil biomass with little loss to streams draining Arctic tundra in Svalbard, Norway. We are unaware of studies that have characterized the isotopic composition of permafrost NO_3^-, but it is likely a mixture of atmospheric and microbial NO_3^- inputs incorporated into ice during permafrost formation.

The main objective of this study was to use dual measurement of N isotopes ($\delta^{15}N$) and oxygen (O) isotopes ($\delta^{18}O$) in NO_3^- to constrain NO_3^- sources in the tundra environment of Barrow, Alaska. NO_3^- isotopes were measured in spring snowmelt and in active layer (soil layer above permafrost that undergoes seasonal thaw) pore water from polygonal terrain and from drainages on the broader surrounding landscape. A secondary goal of our study was to measure the isotopic composition of permafrost NO_3^- and to determine if the NO_3^- dual isotope approach could potentially be used as an indicator of permafrost thaw due to warming. As such, NO_3^- isotopes were measured in both textural permafrost ice (ice with high sediment/peat to ice ratio; all permafrost ice not classified as massive ice/ice wedges) and massive permafrost ice (e.g., ice wedges). If the dual NO_3^- isotope signatures of different NO_3^- sources and microbially related N transformation processes are distinct in a tundra setting, these measurements, along with concentration data, could be used to track NO_3^- flow in the environment and to constrain models of N cycling and mass balance. This technique could be particularly useful in settings where warming is affecting permafrost thaw, leading to increased decomposition of SOM and alterations to the N cycle.

2. Materials and Methods

2.1. Study Site

The study site is located at the Barrow Environmental Observatory (BEO) and surrounding environments on Alaska's North Slope (Figure 1). The average depth of the active layer, the layer of soil subjected to annual freeze/thaw cycles, is typically <0.5 m. Soils are classified as typic histoturbels and aquiturbels [*Bockheim et al*., 1999]. The landscape is characterized as coastal wet sedge tundra [*Shaver et al*., 1992] and is underlain by continuous permafrost, which inhibits drainage leading to high water tables and suboxic soils in much of the landscape [*Lipson et al*., 2012]. The presence of continuous permafrost, annual freezing and thawing of the active layer, and long-term growth and melting of ice in permafrost result in a thaw lake/drained thaw lake basin (DTLB) landscape with areas of polygonal terrain [*Hussey and Michelson*, 1966;

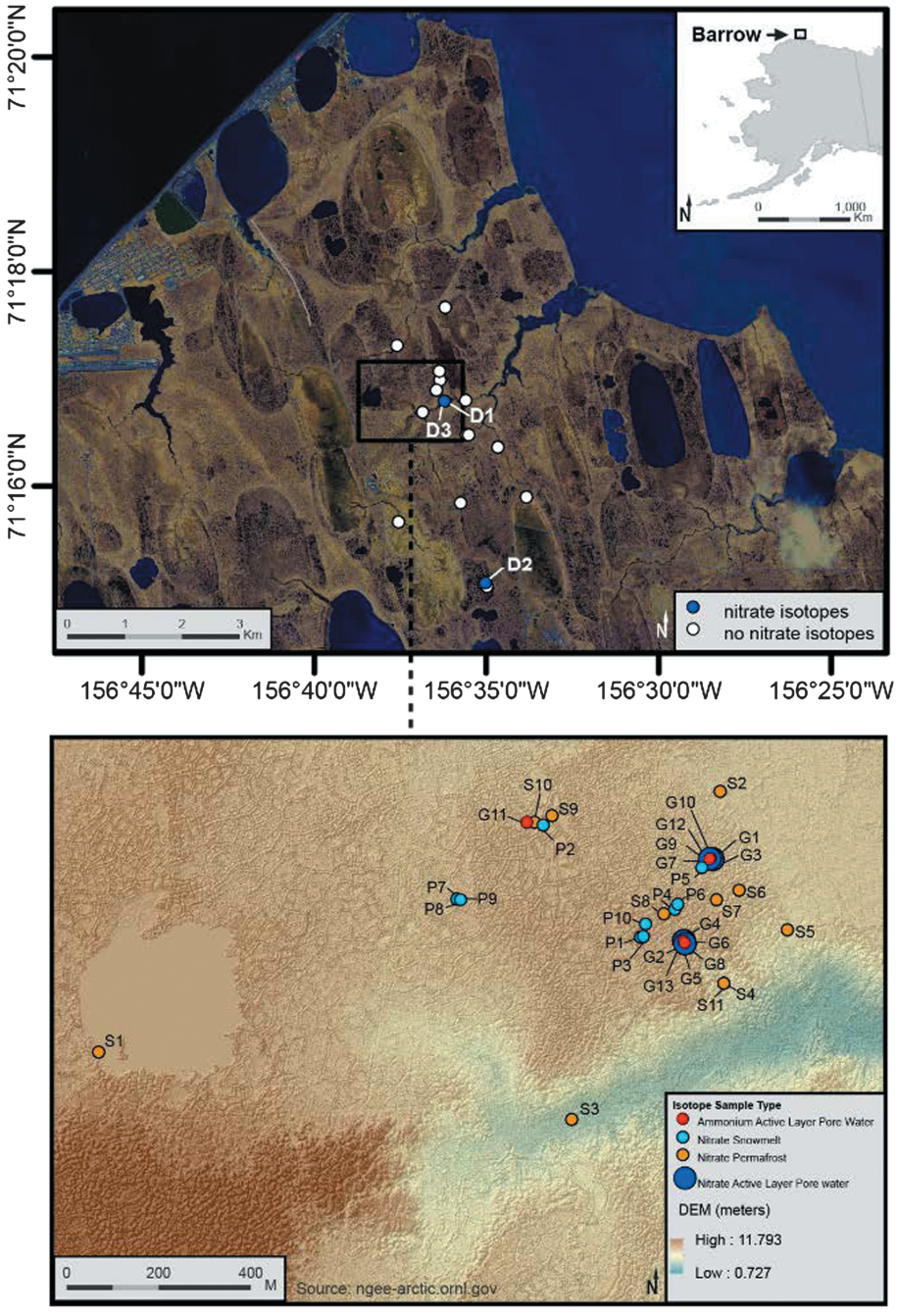

Figure 1. Map showing locations of samples (upper) on broader landscape and (lower) in an area of intensive study (dominated by polygonal terrain). Blue dots in the upper panel show locations where NO_3^- isotope analyses were obtained from active layer pore water. Locations with white dots yielded insufficient water or had insufficient NO_3^- for isotopic analysis. The lower panel shows locations of snowmelt, permafrost, and active layer pore water isotope samples in the intensively studied area of polygonal terrain. Location IDs correspond to those in supporting information Table S1.

Billings and Peterson, 1980; *Jorgenson and Shur*, 2007]. The broad landscape is characterized by hydrogeomorphic features such as ponds, active thaw lakes, different aged DTLBs, interstitial tundra, and drainages leading to the Beaufort and Chukchi Seas [*Hinkel et al*., 2003; *Hinkel et al*., 2005; *Hinkel et al*., 2007; *Lara et al*., 2015]. Patterned polygonal ground, composed of low-centered, flat-centered, and high-centered ice-wedge polygons, is also prominent in the landscape, particularly in interstitial tundra and older DTLBs [*Hussey and Michelson*, 1966; *Hinkel et al*., 2003; *Lara et al*., 2015]. Photos and cross-section diagrams of high- and low-centered polygons,

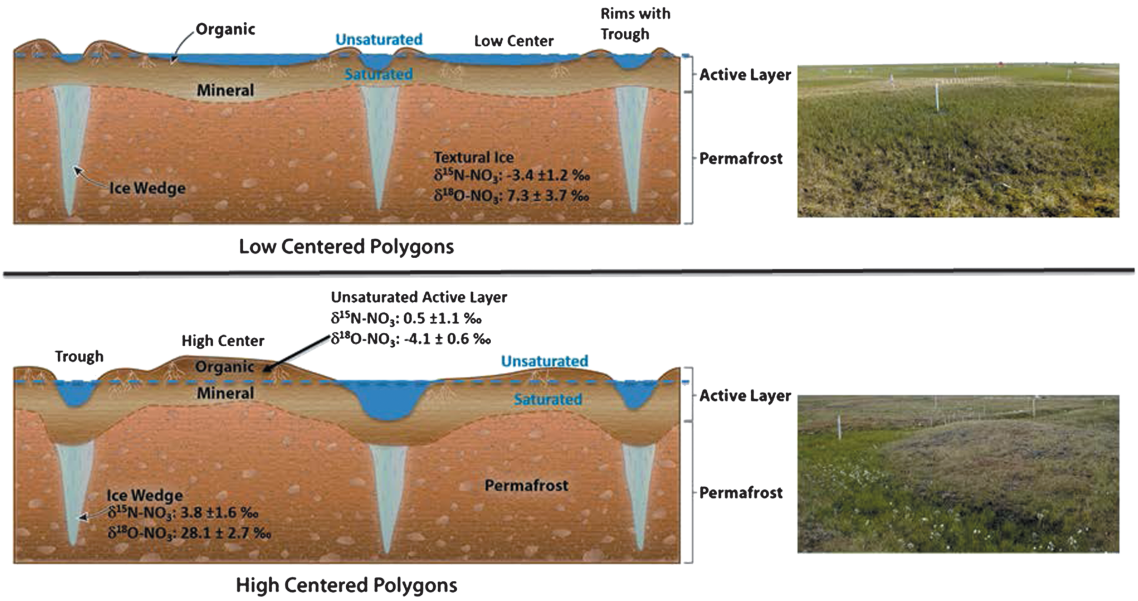

Figure 2. Cartoon cross section of (upper) low-centered and (lower) high-centered polygons with field photos (relief in the high-centered polygon photo is approximately 1 m). Average (± standard error of the mean) values for $\delta^{15}N$ and $\delta^{18}O$ of NO_3^- are shown for the unsaturated active layer pore water of high-centered polygons and for textural and massive permafrost ice. The blue-dashed line in each panel shows the approximate location of soil saturation, with microtopography above the line representing unsaturated conditions. Areas of solid blue in topographic depressions represent standing water. Base figure courtesy of Yuxin Wu and Susan Hubbard.

with typical areas of soil saturation noted along with permafrost features, are shown in Figure 2. Low-centered polygons have low, wet centers and raised rims, with shallow troughs between the rims, with the rims and troughs occurring above massive ice wedges (Figure 2). As ice wedges degrade, there is a resulting topographic inversion in which deeper and wider wet troughs form above degrading ice wedges and surround slightly raised and drier high centers [e.g., *Jorgenson et al.*, 2006] (Figure 2). High-centered polygons in Barrow may also preferentially form in areas of higher elevation topography (interstitial tundra in areas lacking evidence for thaw lake cycles) and areas that have more developed surface drainage patterns to drain water from the troughs above degrading ice wedges [*Hussey and Michelson*, 1966].

2.2. Water Samples From Polygonal Terrain and Drainages

A total of 184 surface water and active layer pore water samples were collected from an area of significant polygon development and from drainages on the broader surrounding landscape for determination of NO_3^- concentrations during the summers of 2012 and 2013. Samples were taken from a total area covering approximately 3 km by 5 km (Figure 1). Active layer pore water sample depths ranged from approximately 5 to 57 cm from the soil surface. A subset of 24 active layer pore water samples in polygonal terrain and surrounding drainages yielded sufficient sample volume and NO_3^- concentrations (see supporting information) for analysis of $\delta^{15}N$ and $\delta^{18}O$ of NO_3^- (supporting information Table S1 and Figure 1). These isotopic results are the primary focus of the study.

Two sets of surface and active layer pore water samples were collected. Samples were collected from troughs and centers of high- and low-centered polygons (Figure 2), herein defined as "polygonal" samples. High- and flat-centered polygons are not differentiated, as both tend to have slightly elevated, more oxic centers. Additionally, in 2013, surface and active layer pore water samples were collected from the periphery of drainages (i.e., streams and ponded areas in channels) in and around the BEO (Figure 1 and supporting information Table S1), herein defined as "drainage" samples. Samples from drainages were typically collected from three depths at each location, including (1) adjacent surface waters, (2) shallow subsurface pore waters (up to 15 cm depth from the surface; soils are commonly organic rich), and (3) at the frost table (bottom of the unfrozen active layer at the time of sampling; soils are often mineral rich and silty in texture; $<$60 cm from the surface; supporting information Table S1).

Surface waters were collected as grab samples in 1 L bottles (HDPE, Nalgene). Subsurface active layer pore waters from polygonal terrain and drainages were collected using a combination of techniques.

For saturated shallow organic-rich soils, stainless steel drive points (Solinst; 2.1 cm inner diameter) were installed and water was pumped into 1 L bottles (HDPE, Nalgene) using a hand-pump vacuum or peristaltic pump (Masterflex). Macro-rhizons [*Seeberg-Elverfeldt et al*., 2005] were more effective for extracting water from deeper saturated soils at the frost table. Macro-rhizon samplers were installed into soils, and pore waters were extracted within 2 h into 60 mL syringes. Passive capillary fiberglass samplers (wick samplers) [*Frisbee et al*., 2010a; *Frisbee et al*., 2010b], along with macro-rhizon samplers, were used to sample pore waters from the unsaturated soil in the centers of high-centered polygons. Wicks were installed at 5 cm depth in the organic horizon and 20 cm depth in the mineral horizon. Additionally, active layer wells made from slotted polyvinyl chloride (PVC) pipes (10 cm diameter) were installed in the BEO intensive sampling area during the summer of 2012. Multilevel samplers (MLS; Margan, Netanya, Israel) were deployed in the PVC wells. The MLS consisted of a solid PVC rod, which was drilled to receive horizontally oriented 40 mL cylindrical diffusion cells every 10 cm depth. The cells were filled with deionized water and sealed with 0.2 μm nylon membranes. The cells were isolated by depth in the well casing with neoprene seals at 10 cm depth intervals [*Crenshaw et al*., 2010]. Solute equilibration was allowed to proceed for a minimum of 1 month. Subsurface samples for NO_3^- isotopic analyses were collected by macro-rhizons, diffusion cells, or passive wicks (supporting information Table S1), which have been shown to provide representative soil pore water chemistry [*Gee et al*., 2003; *Feaga and Selker*, 2004; *Seeberg-Elverfeldt et al*., 2005; *Frisbee et al*., 2010a; *Frisbee et al*., 2010b; *Crenshaw et al*., 2010]. Quantitative recovery of solutes reduces or eliminates the potential for isotopic fractionation associated with sampling.

Surface and pore water samples were filtered (0.45 μm) and stored on ice packs in the field and then frozen until analyzed at the Geochemistry and Geomaterials Research Laboratory, Los Alamos National Laboratory (Los Alamos, NM, USA). NO_3^- and NH_4^+ concentrations were measured where sufficient sample volume was available (see supporting information for analytical details). Similarly, NO_3^- and NH_4^+ isotopes ($\delta^{15}N$ and $\delta^{18}O$, and $\delta^{15}N$, respectively) were measured for samples with sufficient sample volume and NO_3^- and NH_4^+ concentrations (see supporting information for analytical details). The $\delta^{15}N$ of DON was also measured on a subset of samples. Water isotopes ($\delta^{18}O$ and $\delta^{2}H$) were measured on all samples except those collected by the MLS, the cells of which are initially filled with deionized water, thereby rendering such samples unusable for water isotopic analysis.

2.3. Snowmelt

Freshly melted, ponded snowmelt and snowmelt runoff samples were collected as daily grab samples from 11 locations for 14 consecutive days during the brief 2 week snowmelt period (from 30 May 2013 through 13 June 2013), with the exception of one location where samples were not collected on 7 June 2013. One additional snow sample collected in May of 2013 prior to snowmelt was also analyzed for NO_3^- concentrations and isotopes. A total of 153 snow samples were measured for NO_3^- concentrations. Eleven samples with the highest NO_3^- concentrations (representing 7 of the 11 locations; and the additional snow sample) were measured for NO_3^- isotopes (supporting information Table S1). The isotopic composition of dry or wet deposition of atmospheric NO_3^- during the growing season has not been determined for the site.

2.4. Permafrost and Active Layer SOM

Permafrost soil cores were excavated from a range of microtopographic features (see "Polygonal Type" and "Location" in Table 1) in and around the BEO [cores were obtained as described by *Roy Chowdhury et al*., 2015, or by using a handheld SIPRE auger system] during April of 2012 and April and May of 2013. Ice NO_3^- concentrations and isotopes were measured on a subset of these samples. Details on core subsampling and sample preparation are provided in the supporting information. Water isotopes were also determined for those permafrost samples amenable to NO_3^- isotopic analysis. Water isotope from massive ice samples were measured by conventional isotope ratio mass spectrometry (IRMS), while water isotopes from textural ice were measured by equilibration of thawed core samples with dry air in plastic bags and subsequent analysis by cavity ring down spectroscopy [*Lis et al*., 2008].

$\delta^{15}N$ of SOM was measured for 50 samples collected from soil cores taken from the active layer as part of Next-Generation Ecosystem Experiment (NGEE)-Arctic vegetation studies performed by Oak Ridge National Laboratory (ORNL) researchers (supporting information Table S2).

Table 1. NO_3^- Concentrations of Permafrost Ice Samples and Sample Site Characteristics Including Microtopography (Polygonal Type and Location), Sample Depth From the Surface, and Ice Type

ID	Polygonal Type	Location	Depth (cm)	NO_3^- (mg L^{-1})	Ice Type	NO_3^- Isotopes Measured?
NGADG 0048-3b	High-centered polygon	Trough	50–60	0.69	Massive ice	Yes
NGADG 0017-3	Low-centered polygon	Center	53.5–93	1.80	Massive ice	Yes
NGADG 0048-3	High-centered polygon	Trough	50–60	0.53	Massive ice	Yes
NGADG 0043-3	High-centered polygon	Center	50–70	2.56	Massive ice	Yes
BD_001_WI_3	High-centered polygon	Center	14–16	0.28	Textural ice	Yes
BD_001_CN_3	High-centered polygon	Center	59–62	0.18	Textural ice	Yes
BD_001_N_1	High-centered polygon	Center	83–86.5	<0.01	Textural ice	No
BD_002_N_1	High-centered polygon	Trough	50–52	0.16	Massive ice	Yes
BD_004_N_1	High-centered polygon	Trough	39–41	<0.01	Textural ice	No
BD_005_N_1	High-centered polygon	Rim	52–58	0.14	Massive ice	Yes
BD_06_N_1	High-centered polygon	Center	79–84	0.23	Textural ice	Yes
DTLB_38_N_1	Low-centered polygon	Rim	74–77	0.21	Textural ice	Yes
DTLB_39_N_1	Low-centered polygon	Trough	45–48	<0.01	Textural ice	No
DTLB_40_N_1	Low-centered polygon	Center	77–79	<0.01	Textural ice	No
DTLB_40_CN_4	Low-centered polygon	Center	73–77	0.19	Textural ice	Yes
AB_117_N_1	High-centered polygon	Center	88–89.5	<0.01	Textural ice	No
AB_117_WI_4	High-centered polygon	Center	86–88	0.52	Textural ice	Yes
AB_117_WI_3	High-centered polygon	Center	66–68	0.37	Textural ice	Yes

2.5. Chemical and Isotopic Analysis

Detailed descriptions of chemical and isotopic analysis methodology for all sample types are provided in the supporting information. NO_3^- concentrations were analyzed by spectrophotometry or ion chromatography. NH_4^+ concentrations were also determined by spectrophotometry. The $\delta^{15}N$ and $\delta^{18}O$ of NO_3^- were measured using a modified version of the microbial denitrification technique described by *Sigman et al.* [2001] and *Casciotti et al.* [2002] with measurement of evolved N_2O in continuous-flow mode using a GV Instruments Isoprime IRMS (GV Instruments, Manchester, UK) coupled to a TraceGas peripheral instrument. DON samples were converted to NO_3^- by alkaline persulfate oxidation and then analyzed for $\delta^{15}N$ using the microbial denitrification technique (supporting information Table S3). Water samples with dissolved NH_4^+ concentrations over 0.5 mg L^{-1} were analyzed for $\delta^{15}N$ using a modification of the diffusion method of *Holmes et al.* [1998] and analyzed for $\delta^{15}N$ on a Thermo Finnigan MAT 253 IRMS coupled to a Costech elemental analyzer. ^{15}N of total soil N was analyzed using continuous-flow IRMS (Integra CN, SerCon, Crewe, UK). Except for textural ice samples, water $\delta^{18}O$ was measured through analysis of CO_2 equilibrated on a GV Instruments Multiflow peripheral instrument. Water vapor equilibrated with textural ice samples in plastic bags was analyzed with a Picarro Water Isotope Analyzer (model L1115-i).

2.6. Statistical Methodology

All statistical analyses were conducted using the R environment (v. 2.14.0, R Core Team, 2013). To assess potential significant differences in NO_3^- and NH_4^+ concentrations across polygonal microtopography, and to test effects of depth and year/season of collection on NO_3^- isotopes, we used a one-way Spearman permutation test with 9999 Monte Carlo simulations to account for the unbalanced statistical design (i.e., an unequal number of samples from different polygonal features, depths, or time points). We additionally made pairwise comparisons to assess specific differences for variables of interest. Any p-values < 0.05 were considered significant. For concentration data, one half of the detection limit was substituted in the case of nondetects for mean and standard error estimates.

3. Results

3.1. Snowmelt NO_3^- Concentrations

A bulk snow sample taken prior to snowmelt had a NO_3^- concentration of 0.5 mg L^{-1}. Snowmelt NO_3^- concentrations ranged from nondetectable (<0.01 mg L^{-1}) to approximately 3 mg L^{-1} (Figure 3), with higher NO_3^- concentrations occurring during early snowmelt. NH_4^+ concentrations in snowmelt were not characterized in this study, but NH_4^+-N concentrations were roughly double NO_3^--N concentrations during snowmelt runoff at a nearby site in 1973 [*Gersper et al.*, 1980, and references therein].

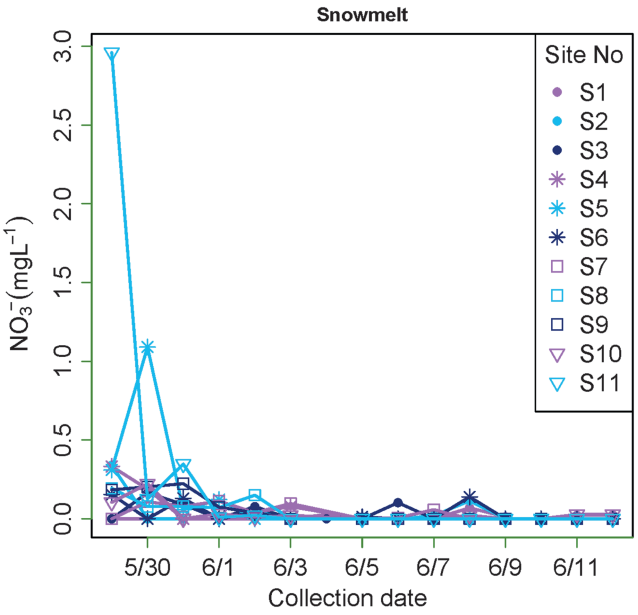

Figure 3. NO_3^- concentration versus date for snowmelt samples (2013). See Figure 1 for site locations.

3.2. Polygonal Terrain and Drainage Active Layer Pore Water NO_3^- and NH_4^+ Concentrations

Within the polygonal terrain, microtopography largely controlled NO_3^- concentrations. Averaged over all depths (including surface water where present), the highest NO_3^- concentrations and greatest frequency of detectable NO_3^- were associated with the centers of high-centered polygons (maximum of ~27 mg L^{-1}, average of ~5 mg L^{-1}; Table 2). NO_3^- was significantly more concentrated in the centers of high-centered polygons relative to the centers of low-centered polygons ($p = 0.027$) and troughs surrounding high-centered polygons ($p = 2.2e^{-16}$). An insufficient number of samples from troughs surrounding low-centered polygons were available for statistical comparison ($n = 4$). These observations are consistent with measurements of plant available NO_3^- using Plant Root Simulators, which showed that NO_3^- availability remained low at all locations and depths (associated with a concurrent vegetation study) throughout the 2013 growing season, with the notable exception of the centers of high-centered polygons. Here NO_3^- availability was very high in the deeper horizons after the soil thawed (Richard J. Norby, Oak Ridge National Laboratory, unpublished data, 2013). The origin of NO_3^- in the centers of high-centered polygons is discussed in section 4.3.

NH_4^+ was most concentrated in surface waters and subsurface active layer pore waters associated with the troughs of high- and low-centered polygons (maximum = 5.32 mg L^{-1}; Table 2), which tend to be saturated and thus more conducive to NH_4^+ stability. NH_4^+ was significantly more concentrated in the troughs of high-centered polygons relative to the centers of high-centered polygons ($p = 0.00134$) and the centers of

Table 2. Average NO_3^- and NH_4^+ Concentrations [for Surface Water (Where Present) and Active Layer Pore Water Combined] of Microtopographic Units of Polygonal Terrain and Drainages[a]

	Nitrate concentrations [NO_3^-] (mg L^{-1} NO_3^-)							
	n	Average			Min	Max	# NO_3^- Detections	% NO_3^- Detections
Polygonal								
High center	25	5.02	±	0.30	<0.01	26.63	20	80
High trough	24	0.01	±	0.00	<0.01	0.08	1	4
Low center	10	0.01	±	0.00	<0.01	0.04	1	10
Low trough	4	0.07	±	0.03	<0.01	0.24	2	50
Drainage	121	0.07	±	0.00	<0.01	2.19	8	7
	Ammonium concentrations [NH_4^+] (mg L^{-1} NH_4^+)							
	n	Average			Min	Max	# NH_4^+ Detections	% NH_4^+ Detections
Polygonal								
High center	17	0.34	±	0.02	<0.1	1.29	8	47
High trough	16	2.04	±	0.10	0.03	5.32	15	93
Low center	9	0.41	±	0.06	<0.1	1.75	7	78
Low trough	2	0.76	±	0.40	0.19	1.33	2	100
Drainage	116	0.04	±	0.00	<0.1	2.86	4	3

[a]Sampling frequency, average, standard error, and minimum and maximum values are shown.

Table 3. NO_3^- Isotopes ($\delta^{15}N$ and $\delta^{18}O$) for the Different Sample Types (Mean and Standard Error)[a]

		NO_3^- (mg L^{-1})		$\delta^{15}N$-NO_3^-		$\delta^{18}O$-NO_3^-	
Location	*n*	Mean	SE	Mean	SE	Mean	SE
High-centered polygon active layer pore water (~5–20 cm)	19	8.0	1.7	0.5	1.1	−4.1	0.6
Snowmelt	11	0.6	0.2	−4.8	1.0	70.2	1.7
Drainage active layer pore water	5	1.1	0.2	7.9	2.3	23.9	3.6
Permafrost	13	0.6	0.2	0.0	1.4	16.3	4.6

[a]Concentration data refer to only those samples on which NO_3^- isotopes were measured.

low-centered polygons ($p = 2e^{-4}$). An insufficient number of samples were available from troughs surrounding low-centered polygons for statistical comparisons.

Only 7% of surface water and subsurface pore water samples from the active layer of drainages had detectable NO_3^-, with average values over all depths (including surface waters) of 0.07 mg L^{-1} (Table 2). Five active layer pore water from three locations were measured for NO_3^- isotopes (locations D1, D3, and D2; supporting information Table S1 and Figure 1). Locations D1 and D3 are in a small drainage that drains directly from an area of high-centered polygons within the NGEE intensive study site. Location D2 is immediately adjacent to a pond located in an ancient DTLB (2000–5500 BP) [*Hinkel et al.*, 2003] with no detectable external surface drainage. NH_4^+ concentrations in surface water and active layer pore waters of drainages were typically less than detection, with a 3% detection frequency (Table 2).

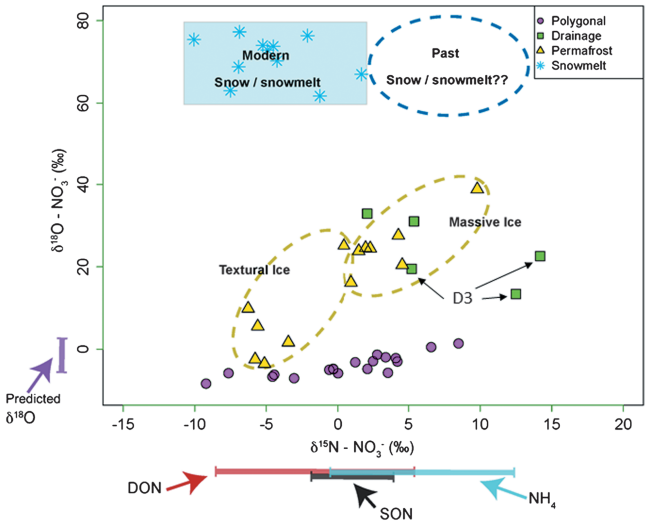

Figure 4. $\delta^{15}N$ versus $\delta^{18}O$ of snowmelt, permafrost, and active layer pore water NO_3^-. The possibility that older, pre-industrial snowmelt may have had a higher $\delta^{15}N$ signature relative to modern snowmelt is shown as a dashed blue oval adjacent to the modern snowmelt field (blue-shaded box). $\delta^{15}N$ ranges of reduced N sources are shown below the *x* axis [soil organic nitrogen (SON), dissolved organic nitrogen (DON), and NH_4^+]. Predicted $\delta^{18}O$ of NO_3^- from nitrification is shown adjacent to the *y* axis (see section 4.1 for explanation of predicted values). The isotopic composition of NO_3^- from the centers of high-centered polygons (pink circles) is generally well constrained by the measured range of $\delta^{15}N$ of reduced sources and the predicted $\delta^{18}O$ range of microbially produced NO_3^-, indicating a microbial origin. Permafrost NO_3^- (yellow triangles) has been subdivided into textural and massive ice and plots at intermediate $\delta^{18}O$ values between microbial NO_3^- and snowmelt NO_3^-. NO_3^- from active layer pore waters of drainages (green squares) could be a mixture of sources and may have been affected by denitrification (see section 4.5). Samples from drainage location D3 are identified as they are specifically discussed in the main text (see section 4.5).

3.3. Permafrost NO_3^- Concentrations

NO_3^- was detected in permafrost samples comprising both massive ice (most likely representing ice wedges) and textural ice, with a maximum concentration of 2.56 mg L^{-1} (Table 1). Based on our limited sample set, concentrations were not associated with polygon type (high versus low center), polygon features (trough, center, and rim), or permafrost ice texture (massive versus textural ice) (Table 1). NH_4^+ concentrations in permafrost ice were not determined.

3.4. $\delta^{15}N$ and $\delta^{18}O$ of NO_3^-

For samples where NO_3^- isotopes were measured (supporting information Table S1), NO_3^- concentrations in active layer pore water averaged 8.0 ± 1.7 mg L^{-1} in high-centered polygons and 1.1 ± 0.2 mg L^{-1} in drainages. Average NO_3^- concentrations were 0.6 ± 0.2 mg L^{-1} in both snowmelt and in permafrost (Table 3). The $\delta^{15}N$ of NO_3^- across all samples ranged from −10.1‰ (bulk snow) to 14.2‰ (active layer pore water in a drainage) (Figure 4 and supporting information Table S1). The $\delta^{18}O$ of NO_3^-

was highly variable, ranging from −8.4‰ (active layer of high-centered polygon) to 77.3‰ (snowmelt) (Figure 4 and supporting information Table S1). The data show distinct NO_3^- isotopic groupings for snowmelt and active layer pore water samples collected from high-centered polygons, primarily based on large differences in $\delta^{18}O$ [Figure 4 and Table 3; $\delta^{18}O$ mean of 70.2 ± 1.7‰ (standard error of the mean) for snowmelt versus −4.1 ± 0.6‰ for active layer pore water samples from high-centered polygons]. Permafrost ice had similar $\delta^{15}N$ values to active layer pore water samples from high-centered polygons and snowmelt, but had more variable $\delta^{18}O$ values intermediate to polygonal NO_3^- and snowmelt (Figure 4 and Table 3; $\delta^{18}O$ mean of 16.3 ± 4.6‰). When considered separately as massive ice versus textural ice, the data form groupings with slight overlap (Figure 4) and have mean $\delta^{15}N$ and $\delta^{18}O$ values of 3.8 ± 1.6‰ and 28.1 ± 2.7‰, respectively, for massive ice and $\delta^{15}N$ and $\delta^{18}O$ values of −3.4 ± 1.2‰ and 7.3 ± 3.7‰, respectively, for textural ice (Figure 2). The isotopic composition of active layer pore waters from drainages was less distinctly grouped (tightly clustered), with 2–3 samples having isotopic signatures similar to permafrost, and 2–3 samples with NO_3^- isotopic signatures dissimilar to other sample types (Figure 4). Table 3 shows means and standard errors for $\delta^{15}N$ and $\delta^{18}O$ of NO_3^- for all isotope samples. All polygonal terrain samples measured for $\delta^{15}N$ and $\delta^{18}O$ of NO_3^- came from the centers of high-centered polygons. Insufficient NO_3^- was available for NO_3^- isotopic analyses from troughs and low-centered polygons. In addition to being provided as supporting information, isotope data and associated sample information are archived on the NGEE data portal as *Heikoop and Throckmorton* [2015].

4. Discussion

4.1. Isotopic Composition of Potential NO_3^- Sources

NO_3^- in tundra soils of the BEO is most likely derived from atmospheric deposition, decomposition, ammonification and nitrification of organic matter, and possibly permafrost thaw. The potential isotopic composition of these sources is considered in this section.

Wet atmospheric NO_3^- (HNO_3 and aerosol NO_3^-) deposition is estimated to be less than 25 mg N^- m^{-2} yr^{-1} [*Dentener et al.*, 2006] on the Arctic Coastal Plain. Atmospheric NO_3^- at high latitude in the Northern Hemisphere, as measured directly from aerosol samples and precipitation and indirectly from snowpacks absent post-depositional isotopic fractionation, has $\delta^{15}N$ of approximately −40‰ to 15‰ and $\delta^{18}O$ of approximately 60‰ to 85‰ [*Hastings et al.*, 2004; *Heaton et al.*, 2004; *Wynn et al.*, 2007; *Tye and Heaton*, 2007; *Morin et al.*, 2008; *Ansari et al.*, 2013; *Louiseize et al.*, 2014; *Nowak and Hodson*, 2014]. Remarkable seasonal variability in $\delta^{15}N$ of atmospheric NO_3^- on the order of 45‰ has been observed at Alert, Nunavut, Canada [*Morin et al.*, 2008]. Such seasonal variations at high latitudes have been related to local production and long-range atmospheric transport of NO_3^-, physicochemical atmospheric processes, and photochemically induced emissions of reactive N from the snowpack [e.g., Blunier *et al.*, 2005; *Savarino et al.*, 2007; *Morin et al.*, 2008]. It is important to note that if atmospheric NO_3^- is assimilated by plants or microbes, the distinct atmospheric $\delta^{18}O$ signature will be eliminated during NO_3^- reduction and assimilation into organic matter. While not a direct atmospheric NO_3^- input, the N_2 fixation flux at Barrow is estimated at 70 mg N m^{-2} yr^{-1} [*Alexander and Schell*, 1973]. N_2 fixation would produce organic matter with $\delta^{15}N$ close to 0‰, that when mineralized and nitrified would yield NO_3^- with $\delta^{15}N$ of approximately 0‰.

In a N limiting environment, N isotopic fractionation during mineralization and nitrification is likely negligible, and the range in $\delta^{15}N$ of NO_3^- should reflect that of reduced sources [*Tye and Heaton*, 2007; *Ansari et al.*, 2013]. During nitrification, it is commonly assumed that one NO_3^- oxygen is derived from atmospheric oxygen ($\delta^{18}O$ of 23.4‰) and two oxygens are from pore water [e.g., Kendall, 1998; *Ansari et al.*, 2013]. While several factors can confound this relationship [*Xue et al.*, 2009; *Ansari et al.*, 2013; *Nowak and Hodson*, 2014], it is a good approximation for the $\delta^{18}O$ of NO_3^- derived from microbial nitrification.

To the best of our knowledge, the NO_3^- isotopic composition of permafrost in the Barrow area has not been previously defined.

4.2. Source of NO_3^- in Snow/Snowmelt

The isotopic composition of NO_3^- in snow and snowmelt samples collected from the BEO was consistent with reports of atmospheric N from High Arctic settings (Figure 4; section 4.1). While isotopic fractionation of water isotopes during snowmelt has been reported [*Lee et al.*, 2010], we are unaware of any NO_3^- isotope

fractionation associated with the melting process that may result in different isotopic compositions early in snowmelt versus later in snowmelt. As spring snowmelt at Barrow is rapid and quantitative, it is unlikely that any such fractionation would be expressed in the snowmelt runoff NO_3^- pool. Additionally, our results showed no obvious temporal trends during the snowmelt period, no correlations between $\delta^{15}N$ and $\delta^{18}O$ of snowmelt NO_3^-, and no values outside of the expected range for atmospheric NO_3^- that would suggest significant microbial processing (either nitrification or denitrification) during snowmelt (supporting information Table S1). These results indicate preservation of the NO_3^- isotopic signature of snow/snowmelt during the snowmelt period.

Based on the NO_3^- concentration time series presented in Figure 3, there was an initial flush of NO_3^- that accumulated in snow during the winter from atmospheric deposition. Similar rapid declines in NO_3^- concentrations during and immediately following snowmelt at Barrow have been noted [*Gersper et al.*, 1980]. In better-drained portions of the landscape, this nutrient pulse may be exported from the system by lateral runoff because of low microbial and plant activity during snowmelt [*Hobbie et al.*, 2002; *Iversen et al.*, 2015]. Snowmelt samples in the current study were collected in relatively well-drained interstitial tundra (Figure 1), suggesting that much of the NO_3^- contained within snow may have been lost from the system via lateral drainage [cf. Gersper *et al.*, 1980].

4.3. Source of NO_3^- in Polygonal Terrain

NO_3^- from the centers of high-centered polygons had $\delta^{15}N$ values ranging from −9.2‰ to +8.5‰ and $\delta^{18}O$ values ranging from −8.4‰ to +1.4‰, consistent with microbial mineralization and nitrification of reduced N [*Ansari et al.*, 2013]. The range in $\delta^{15}N$ of NO_3^- for polygonal active layer pore waters corresponds with that of DON, soil organic nitrogen (SON), and NH_4^+ (Figure 4 and supporting information Tables S1–S3). Figure 4 also shows the predicted range of $\delta^{18}O$ of microbial NO_3^- based on the $\delta^{18}O$ of water of 31 active layer samples from polygonal terrain (range of −20.1‰ to −8.0‰). Given uncertainties in prediction assumptions and the $\delta^{18}O$ of pore water at the time of nitrification, the predicted $\delta^{18}O$ range for polygonal NO_3^- corresponds very closely to measured $\delta^{18}O$ of polygonal NO_3^-, further suggesting a microbial origin.

No statistically significant relationships were found between $\delta^{15}N$ and $\delta^{18}O$ of NO_3^- from high-centered polygons and sampling depth, month, or year of collection. We hypothesize that the variation in $\delta^{15}N$ and $\delta^{18}O$ of NO_3^- is a function of different reduced sources of N being mineralized and nitrified at different times of the year in pore waters with changing seasonal $\delta^{18}O$ signatures. Much higher temporal resolution sampling would be necessary to fully address this hypothesis. The apparent trend (i.e., positive slope) in NO_3^- isotope data from high-centered polygons is discussed in the context of N loss processes in section 4.6. It is interesting that NH_4^+ has higher $\delta^{15}N$ than other reduced N sources. This may be due to Rayleigh fractionation associated with incomplete consumption during plant assimilation and nitrification. Under such circumstances, N isotopic fractionation associated with nitrification could be expressed. However, any such fractionation is minimal given the strong overlap between $\delta^{15}N$ of reduced N sources and NO_3^- produced from nitrification (Figure 4). NO_3^- produced by nitrification is unlikely to undergo significant N isotopic fractionation as a result of plant and microbial uptake/immobilization of DIN because it is nearly quantitatively consumed as a limiting nutrient [*Shaver et al.*, 1992].

Mineralization and nitrification rates are affected by soil moisture, soil temperature, organic matter quality and quantity, nutrient availability, and the availability of oxygen versus alternative electron acceptors [e.g., *Nadelhoffer et al.*, 1991; Shaver et al., 1992; *Hobbie*, 1996; *Hobbie et al.*, 2002; *Weintraub and Schimel*, 2003; *Mack et al.*, 2004; *Weintraub and Schimel*, 2005; *Schuur et al.*, 2008; *Lipson et al.*, 2012]. In contrast to aerobic environments, SOM decomposition rates are 5 to 10 times slower in anaerobic environments where decomposition relies on alternate terminal electron acceptors [*Schuur et al.*, 2008]. Patterned ground features are known to alter N cycling at local scales [*Kelley et al.*, 2012], though not always in predictable fashions. For example, contrary to their expectations, *Biasi et al.* [2005] found lower N pools and mineralization rates in the drier, warmer hummocks of hummock tundra in Siberia, which they attributed to differences in factors such as localized variations in plant functional types between hummocks and inter-hummock areas and lateral transport of N from hummocks to surrounding depressions. In the present study, however, the occurrence of NO_3^- is more likely controlled by soil moisture and redox conditions. Multiple lines of evidence (Eh and dissolved O measurements, water table heights, volumetric water content, surface geophysical measurements, LiDAR interpretation of drainage potential, and concentrations of oxyanions)

demonstrate more oxidizing soil conditions in the slightly raised topography of polygon rims and high centers at the study site [e.g., *Gersper et al.*, 1980; *Engstrom et al.*, 2005; *Lipson et al.*, 2010; *Zona et al.*, 2011; *Lipson et al.*, 2012; *Hubbard et al.*, 2013; *Lipson et al.*, 2013; *Newman et al.*, 2015]. Ongoing monitoring of growing season volumetric water content (VWC) in soil pits in the BEO has shown that active layer soils at 10–5 cm depth in the centers of high-centered polygons are drier (VWC ~30–35%) than deeper active layer soils (VWC of ~50% at 0.50 m in the same pit) (see NGEE_BRW_B at http://lapland.gi.alaska.edu/vdv/vdv_historical.php?station_id=−1&page_id=−1&direct=0). These soils are also drier than those in low-centered polygons. Metagenomics analyses demonstrate high nitrification potential of microbial populations in drier polygon features such as high-centered polygons [Neslihan Taş, Lawrence Berkeley National Laboratory, personal communication, unpublished data, 2014].

There is no evidence for snowmelt-related NO_3^- in active layer pore waters of high-centered polygon centers. The lack of a snowmelt signal may reflect the fact that any snowmelt NO_3^- not transported away through lateral drainage is subsequently assimilated by plants and microbes. The $\delta^{15}N$ signature of snowmelt NO_3^- could be preserved during organic matter synthesis and subsequent decomposition to NO_3^- (assuming little fractionation in a N-limited system), but the initial $\delta^{18}O$ signature of atmospheric NO_3^- would be eliminated when NO_3^- was reduced to organic N. The range in $\delta^{15}N$ of snowmelt NO_3^- is similar to that of NO_3^- in polygonal terrain, suggesting the organic matter synthesis/decomposition pathway could be relevant to the observed isotopic variation in both reduced N sources and NO_3^- derived via nitrification.

Biological waste from animals could also be a potential source of N (and phosphorous) [see Newman *et al.*, 2015] to drier high-centered polygons, where birds tend to perch. Lemmings have been posited as a significant source of N deposition in Barrow [*Batzli et al.*, 1980]. We have observed their predators, snowy owls, perched on high-centered polygons, and *Hussey and Michelson* [1966] identified a nearby soil mound that was "organically enriched with owl droppings." Because owls are carnivores, their droppings are likely to be enriched in ^{15}N due to trophic level effects [*DeNiro and Epstein*, 1981]. Such sources could contribute, upon mineralization and nitrification, to higher NO_3^- concentrations in high-centered polygons and might be a factor in some of the higher polygonal $\delta^{15}N$ values shown in Figure 4, though such relationships remain highly uncertain at this time.

4.4. Sources of NO_3^- in Permafrost

Permafrost thaw associated with soil warming, deepening of the active layer, and localized thermokarst activity could release N to the active layer and to aquatic systems [e.g., *Bowden et al.*, 2008; *Keuper et al.*, 2012; *Harms et al.*, 2014; *Louiseize et al.*, 2014; *Walter et al.*, 2014]. *Lougheed et al.* [2011] suggest that increased NO_3^- concentrations relative to that measured 40 years ago in ponds near Barrow could be due, at least in part, to permafrost thaw. *Keuper et al.* [2012] have called plant available N in the upper permafrost, a "frozen feast" with DIN that could be quickly assimilated upon thaw representing "fast food" and SOM that must first undergo mineralization representing "slow food." DIN may be concentrated in the upper permafrost due to leaching of N from the active layer into the permafrost at the end of summer over decades [cf. *Mackay*, 1983; *Keuper et al.*, 2012] or from incorporation into aggradational ice [cf. *Kokelj and Burn*, 2003].

The NO_3^- isotopic variation in textural versus massive permafrost ice (Figure 4) may be related to such factors as permafrost age, seasonal variation in water sources to permafrost, and short-term and long-term temporal variation in atmospheric NO_3^- source isotopic signatures. Permafrost samples were not radiocarbon dated, but soil organic matter from textural ice from low-centered and high-centered polygons (adjacent to ice wedges) within the intensive study area (Figure 1) all had average ^{14}C ages older than 4000 yr BP (David E. Graham, Oak Ridge National Laboratory, unpublished data, 2013). Ice wedges located immediately below the active layer at Barrow, however, are likely still actively forming and could, therefore, contain some component of modern ice [cf. *Brown*, 1967; *Meyer et al.*, 2010]. The horizontal growth rate of buried ice wedges at Barrow has been estimated at 2 mm yr^{-1} [*Meyer et al.*, 2010]. Using this estimate, pre-industrial ice (i.e., older than ~150 yr BP) might comprise a significant portion of the volume of a 1–2 m wide ice wedge (as estimated from the width of troughs around high-centered polygons and the rims of low-centered polygons). *Meyer et al.* [2010] noted that the (water) isotopic composition of texture ice "may … reflect soil and ground water that was present as initial freezing occurred." As such, much of the NO_3^- in textural ice (and the older portions of permafrost wedge ice) is likely pre-industrial in origin. It is possible that pre-industrial atmospheric NO_3^- inputs at Barrow had higher $\delta^{15}N$ than modern inputs. For example, NO_3^- in Holocene pre-industrial ice from Greenland has

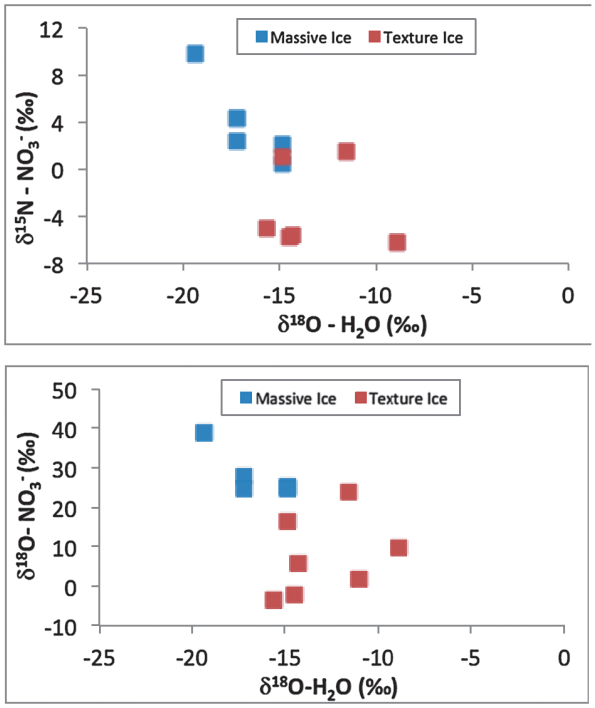

Figure 5. (upper) $\delta^{15}N$ of permafrost NO_3^- versus $\delta^{18}O$ of ice and (lower) $\delta^{18}O$ of permafrost NO_3^- versus $\delta^{18}O$ of ice.

$\delta^{15}N$ approximately 12‰ higher than industrial-era ice and snow [*Hastings et al.*, 2005; *Hastings*, 2010]. The lower $\delta^{15}N$ values of industrial-era ice and snow are attributed to the effect of anthropogenic atmospheric acidity on atmospheric NO_3^- partitioning [*Geng et al.*, 2014]. It is not known if or to what extent current and past atmospheric NO_3^- isotopic signatures at Barrow have varied, but the possibility of a higher pre-industrial $\delta^{15}N$ atmospheric NO_3^- source similar to that seen in Greenland is acknowledged as a dashed field in Figure 4.

Based on water isotope data, numerous studies have demonstrated a winter moisture source for permafrost massive ice and a greater proportion of summer moisture in permafrost textural ice [e.g., *Vaikmäe*, 1989; *Michel*, 1990; *Meyer et al.*, 2010; *Brosius et al.*, 2012]. This suggests that seasonality of NO_3^- sources in these different permafrost sample types will also be a factor. Massive ice wedges form from ground cracking and late-winter/spring snowmelt infiltration and subsequent refreezing in the permafrost zone [*Mackay*, 1974]. Consequently, massive ice wedges have lower water $\delta^{18}O$ and $\delta^{2}H$ consistent with winter precipitation [e.g., *Vaikmäe*, 1989; *Michel*, 1990; *Meyer et al.*, 2010; *Brosius et al.*, 2012]. Seasonality in $\delta^{18}O$ of meteoric waters at the site is distinct with values ranging from −7.5‰ in summer rainfall to −34.4‰ in snow, with a weighted mean annual value of −18.7‰ [*Meyer et al.*, 2010; *IAEA/WMO*, 2015]. Plots of $\delta^{15}N$ and $\delta^{18}O$ of permafrost NO_3^- versus $\delta^{18}O$ of ice are shown in Figure 5. Samples identified as massive ice, likely associated with ice wedges, have lower $\delta^{18}O$ of ice and higher $\delta^{15}N$ and $\delta^{18}O$ of permafrost NO_3^-. Snowmelt from the site, collected in 2012, had an average water $\delta^{18}O$ value of −19‰ (Heather M. Throckmorton Brent D. Newman, Los Alamos National Laboratory, unpublished data, 2012), similar to values for massive ice. It would be expected, therefore, that massive permafrost ice at the site should have a NO_3^- isotopic signature similar to snowmelt NO_3^-.

The $\delta^{18}O$ of NO_3^- in massive ice falls between that of snowmelt (which reflects the NO_3^- isotopic composition of winter atmospheric sources; section 4.2) and microbial sources, suggesting a significant atmospheric component with an additional component of NO_3^- derived from nitrification (Figure 4). The $\delta^{15}N$ of NO_3^- from massive ice, however, is distinctly higher than that of modern snowmelt. To reconcile this fact, NO_3^- isotopic fractionation in the snowpack and seasonal and longer-term temporal variations in the NO_3^- isotopic composition of precipitation are considered.

Spring snowpack NO_x emissions can leave residual NO_3^- enriched in ^{15}N, and seasonal variations in the isotopic composition of Arctic atmospheric NO_3^- occur [*Blunier et al.*, 2005; *Morin et al.*, 2008]. While seasonal atmospheric NO_3^- variations cannot be ruled out as a factor, modern Arctic atmospheric NO_3^- from Alert, Northwest Territories, Canada, produced during the winter and spring has *lower* $\delta^{15}N$ relative to that produced in the summer [*Morin et al.*, 2008]. Moreover, snowpack at Barrow is seasonal and melts completely during a very brief period (~10–14 days) (Figure 3) [*Chapin et al.*, 1980], so any isotopic variation related to winter/spring atmospheric inputs or snowpack NO_x emissions would have been integrated into the snowmelt samples that were analyzed for NO_3^- isotopes and considered as a potential NO_3^- source to massive ice wedges. A possible explanation for higher $\delta^{15}N$ of massive ice relative to modern snowmelt is that pre-industrial atmospheric NO_3^- inputs had higher $\delta^{15}N$ and are a significant component of the

massive ice NO_3^- pool. Overall, while massive ice contains substantial amounts of atmospheric NO_3^-, we propose that much of that NO_3^- may have a different isotopic composition than modern snowmelt NO_3^- due to mixing of modern and pre-industrial sources.

We infer that NO_3^- in textural ice contains a greater component of microbial NO_3^- than massive ice based on similar $\delta^{15}N$ and $\delta^{18}O$ values to microbial NO_3^- from high-centered polygons (section 4.3) and the fact that most samples have $\delta^{18}O$ of NO_3^- that is much lower than that of atmospheric sources (Figure 4). The water isotope signature in textural ice is consistent with a greater component of microbial NO_3^- derived from organic matter decomposition and nitrification during the summer season. We speculate that much of the microbial NO_3^- in textural ice was likely incorporated during initial permafrost formation when soils may have been better drained before the presence of permafrost limited vertical drainage to the extent now observed. It is not surprising that textural ice does not, in general, have a purely "summer" microbial NO_3^- signal as it can be formed partially from winter precipitation [*Vaikmäe*, 1989]. Also, microbial decomposition can occur during winter, even under subzero conditions, due to the presence of liquid water films [*Sturm et al*., 2005]; thus, a microbial component formed in situ in both textural and massive ice is possible. In situ nitrification cannot, however, be the primary signal in massive ice as evidenced by the relatively low $\delta^{18}O$ of water (Figure 5) and higher $\delta^{18}O$ of NO_3^- than either textural ice or modern snowmelt (Figure 4) (see discussion of $\delta^{18}O$ of microbial NO_3^- in section 4.1). The potential effect of denitrification on observed signals is discussed below in section 4.6 on N loss from the system.

There is substantial variation in the NO_3^- isotopic composition of permafrost ice (Figure 4), but were large-scale thaw of the permafrost to occur, this variation would be reduced by hydrologic mixing. The isotopic composition of NO_3^- released from permafrost into the active layer would likely be intermediate between microbial and atmospheric NO_3^- sources, reflecting a mix of the different NO_3^- sources incorporated during formation. This resulting signature would likely be indistinguishable from a mixture of newly deposited atmospheric NO_3^- input to the active layer and microbial NO_3^- formed in situ in the active layer. As noted in section 4.3 and below in section 4.5, however, there is little compelling evidence for preservation of the NO_3^- isotopic signature of direct atmospheric inputs in the thawed active layer due to efficient assimilation by plants and microbes.

4.5. Source of NO_3^- in Active Layer Pore Water of Drainages

Only five samples from active layer pore water yielded sufficient volume and NO_3^- concentrations for isotopic analysis. Two samples from the frost table [locations D1 and D2; drainage from an area of high-centered polygons in interstitial tundra and an ancient DTLB, respectively (Figure 1)] have similar isotopic signatures to that of permafrost (Figure 4). These isotopic values may result from mixing between microbial NO_3^- with the highest observed $\delta^{15}N$ values and modern atmospheric NO_3^- (Figure 4). Alternatively, NO_3^- in these samples could result from localized permafrost thaw. We have no independent evidence for permafrost thaw at these locations, but periodic active layer thickening does occur at the site [*Shiklomanov et al*., 2010; see also *Bockheim and Hinkel*, 2005; *Jorgenson et al*., 2006; and *Raynolds et al*., 2014, for discussion of periodic thawing of the transition layer between the active layer and upper permafrost]. At the time of sampling, the active layer at location D1 was among the deepest measured, at 57 cm (supporting information Table S1). The active layer was not particularly deep at location D2, but of all the locations examined, this ancient DTLB had the most surface water due to lack of external drainage from the basin (sampling occurred adjacent to a pond), potentially increasing the possibility of permafrost degradation due to increased thermal conductivity from standing water within internal drainages [e.g., *Jorgenson et al*., 2010].

The isotopic composition of active layer pore water NO_3^- collected with diffusion cells at location D3 does not exhibit a clear trend with depth (supporting information Table S1), and the data are not well constrained in terms of mixing of the measured NO_3^- sources (Figure 4). One hypothesis to partially explain these data is mixing of NO_3^- from degrading ice wedges and microbial NO_3^-, produced either in situ or transported from the adjacent area of high-centered polygons. The potential effect of denitrification on these data is considered in section 4.6. In any case, the source and cycling of N in these samples remain uncertain.

4.6. Nitrate Loss

The main pathways of N loss in the ecosystem are lateral transport and denitrification. Lateral transport primarily occurs during the approximately 10–14 day long snowmelt season each spring [*Chapin et al*., 1980]

and is expected to be nonfractionating with respect to NO_3^- isotopes. Tundra soils in the BEO are sufficiently reducing to promote methanogenesis [e.g., *Chapin et al*., 1980], so denitrification would also be expected to occur. However, denitrification rates are low [*Chapin et al*., 1980], and the N flux related to denitrification is similar to that of lateral transport, estimated at 0.002 g N m^{-2} yr^{-1} [*Chapin et al*., 1980].

Denitrification results in higher $\delta^{15}N$ and $\delta^{18}O$ values in residual NO_3^- and could, therefore, modify the isotopic signature of NO_3^- sources [*Amberger and Schmidt*, 1987]. For example, *Ansari et al*. [2013] showed isotopic evidence for denitrification within sediments in a glacial system on Svalbard, Norway. If significant denitrification occurs in saturated soils at our study site, this process, along with NO_3^- assimilation, appears to result in NO_3^- concentrations that are not readily amenable to isotopic analysis.

In general, the low NO_3^- concentrations in saturated soils of the study site make it difficult to examine the overall importance of denitrification in the landscape using natural abundance isotopic techniques. It is possible, however, that denitrification may have modified the signals described in sections 4.3. For example, there is an apparent slope of 0.45 in $\delta^{18}O$ versus $\delta^{15}N$ ($p = 2.1e^{-6}$) of high-centered polygonal NO_3^- samples (Figure 4). This trend is suggestive of denitrification [cf. *Ansari et al*., 2013]. However, there was not a corresponding decrease in NO_3^- concentrations with increasing $\delta^{15}N$ of NO_3^- ($p = 0.48$) to support a denitrification trend, but sampling was spatially and temporally heterogeneous and likely does not reflect a single NO_3^- source subject to denitrification along a uniform flow pathway. It is possible that there is intermittent denitrification in high-centered polygon centers during periods of saturation following precipitation events. In this case, denitrification would represent a relatively small isotopic overprint on a primary nitrification signal. The effect would have to be minor as polygonal NO_3^- isotope values are generally consistent with predictions as discussed in section 4.3. Similarly, the NO_3^- isotopic composition of drainage active layer pore waters from location D3 could reflect lateral transport of microbial NO_3^- produced in the adjacent area of high-centered polygons (Figures 1 and 4), followed by percolation and partial denitrification. It is also possible that the higher $\delta^{15}N$ and $\delta^{18}O$ values of massive permafrost ice relative to textural ice (Figure 4) are partially due to denitrification occurring during landscape inundation by snowmelt and subsequent infiltration into ice wedge cracks. The NO_3^- isotopic signature of modern snowmelt, however, is entirely consistent with a primary atmospheric NO_3^- source (Figure 4; section 4.2). Moreover, denitrification cannot explain entirely the isotopic difference between textural and massive ice as the offset in $\delta^{18}O$ relative to $\delta^{15}N$ is significantly greater than can be explained by denitrification alone (Figure 4).

Denitrification in the tundra environment of Barrow is likely best studied with labeled isotope approaches and flux measurements along consistent flow paths.

5. Conclusions

Microbially derived NO_3^- in Barrow active layer pore waters appears to accumulate preferentially in more oxic settings such as the centers of high-centered polygons and is a significant component of textural permafrost ice. Conversely, atmospheric NO_3^- was not clearly and unambiguously identified as a primary, unmodified signal in active layer pore waters, presumably because of lateral transport losses during snowmelt and/or subsequent rapid incorporation by plants and microbes. Rather, in our study area, atmospheric NO_3^- occurs as a primary signal in snow and snowmelt, and was directly assimilated from winter snowmelt as a component of the NO_3^- pool in massive permafrost ice.

Permafrost NO_3^- in the Barrow region (including both massive and textural ice) has an intermediate, highly variable isotopic composition depending on the amount of microbial NO_3^- versus atmospheric NO_3^- incorporated into ice during freezing and aggradation. Upon thaw, permafrost is likely to contribute NO_3^- to the active layer with an isotopic signature intermediate to that of atmospheric NO_3^- inputs and NO_3^- derived from microbial denitrification. Because atmospheric NO_3^- signals appear to be uncommon in active layer soils of N limiting environments, monitoring of frost-table NO_3^- isotopes could provide insight into permafrost thaw and its effect on the active layer N cycle. To better understand the dual NO_3^- isotopic signature of permafrost, additional work is needed across a range of well-dated samples (e.g., from outcrop exposures, excavated ice wedges, and permafrost tunnels) of varying ages, landscape positions, and subject to different NO_3^--related atmospheric and snowpack processes. Future studies should also examine the

persistence of a NO_3^- isotope signature from permafrost melt in different environments such as tundra active layers, streams, and lakes, with different nutrient residence times and degree of N limitation. Such studies would also help determine if the NO_3^- dual isotope approach has utility in reconstructing past NO_3^--related atmospheric processes from records contained in ice wedges.

In addition to identifying NO_3^- sources, NO_3^- isotopes could be applied in tracking the N biogeochemical consequences of landscape evolution associated with warming and permafrost thaw. Future hydrogeomorphic changes in Arctic environments will play an important role in biogeochemical cycles by determining the distribution of surface water and soil moisture, and will have important feedbacks to permafrost degradation [e.g., *Shaver et al.*, 1992; *Engstrom et al.*, 2005; *Smith et al.*, 2005; *Hinzman et al.*, 2005; *Jorgenson et al.*, 2006; *Rowland et al.*, 2010; *Jorgenson et al.*, 2010; *Arp et al.*, 2011; *Grosse et al.*, 2011a; *Grosse et al.*, 2011b; *Hinzman et al.*, 2013; *Kokelj and Jorgenson*, 2013; *Lara et al.*, 2015]. Low elevation, low relief continuous permafrost regions may get wetter due to thermokarst-related subsidence and increased formation of thermokarst lakes [*Smith et al.*, 2005]. Conversely, thaw lakes may be drained as a result of permafrost degradation and erosive processes [*Hinkel et al.*, 2003], and local drying may occur. For example, drying may preferentially occur in slightly higher, better-drained, interstitial tundra. Microtopographic-scale drying could result from topographic inversion of polygonal terrain associated with ice-wedge degradation, which may lead to a transition from low- to high-centered polygons [see *Mackay*, 2000; *Jorgenson and Osterkamp*, 2005; *Jorgenson et al.*, 2006; and the review in *Lara et al.* [2015, and references therein]. The degree of landscape drying versus wetting will also depend on changes in precipitation versus potential evaporation [*Hinzman et al.*, 2005]. Any increase in soil oxygenation would increase nutrient mineralization and nitrification [e.g., *Shaver et al.*, 1992; *Nadelhoffer et al.*, 1991] with possible feedbacks to primary productivity and plant and microbial communities. Conversely, large-scale wetting of the landscape may stimulate denitrification. With so many uncertainties with respect to N cycling in the Arctic, natural abundance NO_3^- isotope techniques should prove useful in assessing changes in N biogeochemistry resulting from the redistribution of water across high-latitude landscapes.

Acknowledgments

Data associated with isotope samples are provided in Tables S1–S3. Concentration data for all other samples can be obtained directly from the corresponding author. This work was performed under the auspices of the Next-Generation Ecosystem Experiments (NGEE Arctic) project, which is supported by the Office of Biological and Environmental Research in the U.S. Department of Energy (DOE)-Office of Science. We wish to thank Garrett Altmann, Deanne Brice, Joanne Childs, Lily Cohen, Michael Hudak, Marvin Gard, Ingrid Slette, and Victoria Sloan for field and laboratory assistance, and UMIAQ, LLC, for logistical support in Barrow. The manuscript benefited greatly from the thorough and constructive comments of two anonymous reviewers. This work has been authored by an employee of Los Alamos National Security, LLC, operator of the Los Alamos National Laboratory under contract DE-AC52-06NA25396 with the U.S. Department of Energy. The United States Government retains and the publisher, by accepting this work for publication, acknowledges that the United States Government retains a nonexclusive, paid-up, irrevocable, worldwide license to publish or reproduce this work or allow others to do so for the United States Government purposes.

References

Alexander, V., and D. M. Schell (1973), Seasonal and spatial variation of nitrogen fixation in the Barrow, Alaska, tundra, *Arct. Alp. Res.*, *5*, 77–88.

Amberger, A., and H. L. Schmidt (1987), The natural isotope content of nitrate as an indicator of its origin, *Geochim. Cosmochim. Acta*, *51*(10), 2699–2705, doi:10.1016/0016-7037(87)90150-5.

Ansari, A. H., A. J. Hodson, T. H. E. Heaton, J. Kaiser, and A. Marca-Bell (2013), Stable isotopic evidence for nitrification and denitrification in a High Arctic glacial ecosystem, *Biogeochemistry*, *113*(1–3), 341–357, doi:10.1007/s10533-012-9761-9.

Arp, C. D., B. M. Jones, F. E. Urban, and G. Grosse (2011), Hydrogeomorphic processes of thermokarst lakes with grounded-ice and floating-ice regimes on the Arctic coastal plain, Alaska, *Hydrol. Process.*, *25*(15), 2422–2438, doi:10.1002/hyp.8019.

Batzli, G. O., R. G. White, S. F. MacLean Jr., F. A. Pitelka, and B. D. Collier (1980), The herbivore-based trophic system, in *An Arctic Ecosystem: The Coastal Tundra at Barrow, Alaska*, edited by J. Brown et al., pp. 335–410, Dowden, Hutchinson and Ross, Stroudsburg, Pa.

Biasi, C., W. Wanek, O. Rusalimova, C. Kaiser, H. Meyer, P. Barsukov, and A. Richter (2005), Microtopography and plant-cover controls on nitrogen dynamics in hummock tundra ecosystems in Siberia, *Arct. Antarct. Alp. Res.*, *37*(4), 435–443, doi:10.1657/1523-0430(2005)037[0435:mapcon]2.0.CO;2.

Billings, W. D., and K. M. Peterson (1980), Vegetational change and ice-wedge polygons through the thaw-lake cycle in Arctic Alaska, *Arct. Antarct. Alp. Res.*, *12*(4), 413–432, doi:10.2307/1550492.

Blunier, T., G. L. Floch, H. W. Jacobi, and E. Quansah (2005), Isotopic view on nitrate loss in Antarctic surface snow, *Geophys. Res. Lett.*, *32*, L13501, doi:10.1029/2005GL023011.

Bockheim, J. G., and K. M. Hinkel (2005), Characteristics and significance of the transition zone in drained thaw-lake basins of the Arctic Coastal Plain, Alaska, *Arctic*, *58*(4), 406–417, doi:10.14430/arctic454.

Bockheim, J. G., L. R. Everett, K. M. Hinkel, F. E. Nelson, and J. Brown (1999), Soil organic carbon storage and distribution in Arctic tundra, Barrow, Alaska, *Soil Sci. Soc. Am. J.*, *63*(4), 934–940, doi:10.2136/sssaj1999.634934.

Bowden, W. B., M. N. Gooseff, A. Balser, A. Green, B. J. Peterson, and J. Bradford (2008), Sediment and nutrient delivery from thermokarst features in the foothills of the North Slope, Alaska: Potential impacts on headwater stream ecosystems, *J. Geophys. Res.*, *113*, G02026, doi:10.1029/2007JG000470.

Brosius, L. S., K. M. W. Anthony, G. Grosse, J. P. Chanton, L. M. Farquharson, P. P. Overduin, and H. Meyer (2012), Using the deuterium isotope composition of permafrost meltwater to constrain thermokarst lake contributions to atmospheric CH_4 during the last deglaciation, *J. Geophys. Res.*, *117*, G01022, doi:10.1029/2011JG001810.

Brown, J. (1967), Tundra soils formed over ice wedges, Northern Alaska, *Soil Sci. Soc. Am. Pro.*, *31*(5), 686–691, doi:10.2136/sssaj1967.03615995003100050022x.

Campbell, D. H., C. Kendall, C. C. Y. Chang, S. R. Silva, and K. Tonnessen (2002), Pathways for nitrate release from an alpine watershed: Determination using $\delta^{15}N$ and $\delta^{18}O$, *Water Resour. Res.*, *38*(5), 1052, doi:10.1029/2001WR000294.

Casciotti, K. L., D. M. Sigman, M. G. Hastings, J. K. Bohlke, and A. Hilkert (2002), Measurement of the oxygen isotopic composition of nitrate in seawater and freshwater using the denitrifier method, *Anal. Chem.*, *74*(19), 4905–4912, doi:10.1021/ac020113w.

Chapin, F. S., III, P. C. Miller, W. D. Billings, and P. Coyne (1980), Carbon and nutrient budgets and their control in coastal tundra, in *An Arctic Ecosystem: The Coastal Tundra at Barrow, Alaska*, edited by J. Brown et al., pp. 458–482, Dowden, Hutchinson and Ross, Stroudsburg, Pa.

Crenshaw, C. L., N. B. Grimm, L. H. Zeglin, R. W. Sheibley, C. N. Dahm, and A. D. Pershall (2010), Dissolved inorganic nitrogen dynamics in the hyporheic zone of reference and human-altered southwestern U. S. streams, *Fund. Appl. Limnol.*, *176*(4), 391–405, doi:10.1127/1863-9135/2010/0176-0391.

Curtis, C. J., C. D. Evans, C. L. Goodale, and T. H. E. Heaton (2011), What have stable isotope studies revealed about the nature and mechanisms of N saturation and nitrate leaching from semi-natural catchments?, *Ecosystems*, *14*(6), 1021–1037, doi:10.1007/s10021-011-9461-7.

Deniro, M. J., and S. Epstein (1981), Influence of diet on the distribution of nitrogen isotopes in animals, *Geochim. Cosmochim. Acta*, *45*(3), 341–351, doi:10.1016/0016-7037(81)90244-1.

Dentener, F., et al. (2006), Nitrogen and sulfur deposition on regional and global scales: A multimodel evaluation, *Global Biogeochem. Cycles*, *20*, GB4003, doi:10.1029/2005GB002672.

Engstrom, R., A. Hope, H. Kwon, D. Stow, and D. Zamolodchikov (2005), Spatial distribution of near surface soil moisture and its relationship to microtopography in the Alaskan Arctic coastal plain, *Nord. Hydrol.*, *36*(3), 219–234.

Feaga, J., and J. Selker (2004), Field measurements of nitrate leaching below Willamette Valley row and mint crops, *Oregon State University Extension Service*, *EM 8851*, pp. 1–7.

Frisbee, M. D., F. M. Phillips, A. R. Campbell, and J. M. H. Hendrickx (2010a), Modified passive capillary samplers for collecting samples of snowmelt infiltration for stable isotope analysis in remote, seasonally inaccessible watersheds 1: Laboratory evaluation, *Hydrol. Process.*, *24*(7), 825–833, doi:10.1002/hyp.7523.

Frisbee, M. D., F. M. Phillips, A. R. Campbell, J. M. H. Hendrickx, and E. M. Engle (2010b), Modified passive capillary samplers for collecting samples of snowmelt infiltration for stable isotope analysis in remote, seasonally inaccessible watersheds 2: Field evaluation, *Hydrol. Process.*, *24*(7), 834–849, doi:10.1002/hyp.7524.

Gee, G. W., Z. F. Zhang, and A. L. Ward (2003), A modified vadose zone fluxmeter with solution collection capability, *Vadose Zone J.*, *2*(4), 627–632, doi:10.2136/vzj2003.6270.

Geng, L., B. Alexander, J. Cole-Dai, E. J. Steig, J. Savarino, E. D. Sofen, and A. J. Schauer (2014), Nitrogen isotopes in ice core nitrate linked to anthropogenic atmospheric acidity change, *Proc. Natl. Acad. Sci. U.S.A.*, *111*(16), 5808–5812, doi:10.1073/pnas.1319441111.

Gersper, P. L., V. Alexander, S. A. Barkley, R. J. Barsdate, and P. S. Flint (1980), The soils and their nutrients, in *An Arctic Ecosystem: The Coastal Tundra at Barrow, Alaska*, edited by J. Brown et al., pp. 219–254, Dowden, Hutchinson and Ross, Stroudsburg, Pa.

Grosse, G., V. Romanovsky, T. Jorgenson, K. W. Anthony, J. Brown, and P. P. Overduin (2011a), Vulnerability and feedbacks of permafrost to climate change, *Eos Trans. AGU*, *92*(9), 73–74, doi:10.1029/2011EO090001.

Grosse, G., et al. (2011b), Vulnerability of high-latitude soil organic carbon in North America to disturbance, *J. Geophys. Res.*, *116*, G00K06, doi:10.1029/2010JG001507.

Harms, T. K., B. W. Abbott, and J. B. Jones (2014), Thermo-erosion gullies increase nitrogen available for hydrologic export, *Biogeochemistry*, *117*(2–3), 299–311, doi:10.1007/s10533-013-9862-0.

Hastings, M. G. (2010), Evaluating source, chemistry and climate change based upon the isotopic composition of nitrate in ice cores, paper presented at PAGES 1st Young Scientists Meeting (YSM)—Retrospective Views on Our Planet's Future, Corvallis, Ore., doi:10.1088/1755-1315/9/1/012002.

Hastings, M. G., E. J. Steig, and D. M. Sigman (2004), Seasonal variations in N and O isotopes of nitrate in snow at Summit, Greenland: Implications for the study of nitrate in snow and ice cores, *J. Geophys. Res.*, *109*, D20306, doi:10.1029/2004JD004991.

Hastings, M. G., D. M. Sigman, and E. J. Steig (2005), Glacial/interglacial changes in the isotopes of nitrate from the Greenland Ice Sheet Project 2 (GISP2) ice core, *Global Biogeochem. Cycles*, *19*, GB4024, doi:10.1029/2005GB002502.

Heaton, T. H. E., P. Wynn, and A. M. Tye (2004), Low $^{15}N/^{14}N$ ratios for nitrate in snow in the High Arctic (79°N), *Atmos. Environ.*, *38*(33), 5611–5621, doi:10.1016/j.atmosenv.2004.06.028.

Heikoop, J. M., and H. M. Throckmorton (2015), Nitrogen concentration and isotope dataset for environmental samples from 2012 and 2013, Barrow, Alaska, NGEE Arctic Data Collection, Carbon Dioxide Information Analysis Center, Oak Ridge Natl. Lab., U.S. Dep. of Energy, Oak Ridge, Tenn., doi:10.5440/1179130.

Hinkel, K. M., W. R. Eisner, J. G. Bockheim, F. E. Nelson, K. M. Peterson, and X. Y. Dai (2003), Spatial extent, age, and carbon stocks in drained thaw lake basins on the Barrow Peninsula, Alaska, *Arct. Antarct. Alp. Res.*, *35*(3), 291–300, doi:10.1657/1523-0430(2003)035[0291:SEAACS]2.0.CO;2.

Hinkel, K. M., R. C. Frohn, F. E. Nelson, W. R. Eisner, and R. A. Beck (2005), Morphometric and spatial analysis of thaw lakes and drained thaw lake basins in the western Arctic Coastal Plain, Alaska, *Permafrost Periglac. Process.*, *16*(4), 327–341, doi:10.1002/ppp.532.

Hinkel, K. M., B. M. Jones, W. R. Eisner, C. J. Cuomo, R. A. Beck, and R. Frohn (2007), Methods to assess natural and anthropogenic thaw lake drainage on the western Arctic coastal plain of northern Alaska, *J. Geophys. Res.*, *112*, F02S16, doi:10.1029/2006JF000584.

Hinzman, L. D., et al. (2005), Evidence and implications of recent climate change in northern Alaska and other Arctic regions, *Clim. Change*, *72*(3), 251–298, doi:10.1007/s10584-005-5352-2.

Hinzman, L. D., C. J. Deal, A. D. McGuire, S. H. Mernild, I. V. Polyakov, and J. E. Walsh (2013), Trajectory of the Arctic as an integrated system, *Ecol. Appl.*, *23*(8), 1837–1868, doi:10.1890/11-1498.1.

Hobbie, S. E. (1996), Temperature and plant species control over litter decomposition in Alaskan tundra, *Ecol. Monogr.*, *66*(4), 503–522, doi:10.2307/2963492.

Hobbie, S. E., K. J. Nadelhoffer, and P. Hogberg (2002), A synthesis: The role of nutrients as constraints on carbon balances in boreal and arctic regions, *Plant Soil*, *242*(1), 163–170, doi:10.1023/A:1019670731128.

Holmes, R. M., J. W. McClelland, D. M. Sigman, B. Fry, and B. J. Peterson (1998), Measuring $^{15}N\text{-}NH_4^+$ in marine, estuarine and fresh waters: An adaptation of the ammonia diffusion method for samples with low ammonium concentrations, *Mar. Chem.*, *60*(3–4), 235–243, doi:10.1016/S0304-4203(97)00099-6.

Hubbard, S. S., et al. (2013), Quantifying and relating land-surface and subsurface variability in permafrost environments using LiDAR and surface geophysical datasets, *Hydrogeol. J.*, *21*(1), 149–169, doi:10.1007/s10040-012-0939-y.

Hussey, K. M., and R. W. Michelson (1966), Tundra relief features near Point Barrow, Alaska, *Arctic*, *19*(2), 162–184, doi:10.14430/arctic3423.

IAEA/WMO (2015), Global network of isotopes in precipitation. The GNIP database. [Available at http://www.iaea.org/water.]

Iversen, C. M., V. L. Sloan, P. F. Sullivan, E. S. Euskirchen, A. D. McGuire, R. J. Norby, A. P. Walker, J. M. Warren, and S. D. Wullschleger (2015), The unseen iceberg: Plant roots in arctic tundra (Tansley review), *New Phytol.*, *205*, 34–58, doi:10.1111/nph.13003.

Jansson, J. K., and N. Tas (2014), The microbial ecology of permafrost, *Nat. Rev. Microbiol.*, *12*(6), 414–425, doi:10.1038/nrmicro3262.

Jorgenson, M. T., and T. E. Osterkamp (2005), Response of boreal ecosystems to varying modes of permafrost degradation, *Can. J. For. Res.*, *35*(9), 2100–2111, doi:10.1139/x05-153.

Jorgenson, M. T., and Y. Shur (2007), Evolution of lakes and basins in northern Alaska and discussion of the thaw lake cycle, *J. Geophys. Res.*, *112*, F02S17, doi:10.1029/2006JF000531.

Jorgenson, M. T., Y. L. Shur, and E. R. Pullman (2006), Abrupt increase in permafrost degradation in Arctic Alaska, *Geophys. Res. Lett.*, *33*, L02503, doi:10.1029/2005GL024960.

Jorgenson, M. T., V. Romanovsky, J. Harden, Y. Shur, J. O'Donnell, E. A. G. Schuur, M. Kanevskiy, and S. Marchenko (2010), Resilience and vulnerability of permafrost to climate change, *Can. J. For. Res.*, *40*(7), 1219–1236, doi:10.1139/X10-060.

Kelley, A. M., H. E. Epstein, C.-L. Ping, and D. A. Walker (2012), Soil nitrogen transformations associated with small patterned-ground features along a North American Arctic transect, *Permafrost Periglac. Process.*, *23*(3), 196–206, doi:10.1002/ppp.1748.

Kendall, C. (1998), Tracing nitrogen sources and cycling in catchments, in *Isotope Tracers in Catchment Hydrology*, edited by C. Kendall and J. J. Mcdonnell, pp. 519–576, Elsevier, Amsterdam.

Keuper, F., P. M. van Bodegom, E. Dorrepaal, J. T. Weedon, J. van Hal, R. S. P. van Logtestijn, and R. Aerts (2012), A frozen feast: Thawing permafrost increases plant-available nitrogen in subarctic peatlands, *Global Change Biol.*, *18*(6), 1998–2007, doi:10.1111/j.1365-2486.2012.02663.x.

Kokelj, S. V., and C. R. Burn (2003), Ground ice and soluble cations in near-surface permafrost, Inuvik, Northwest Territories, Canada, *Permafrost Periglac. Process.*, *14*(3), 275–289, doi:10.1002/ppp.458.

Kokelj, S. V., and M. T. Jorgenson (2013), Advances in thermokarst research, *Permafrost Periglac. Process.*, *24*(2), 108–119, doi:10.1002/ppp.1779.

Lacelle, D., and Y. K. Vasil'chuk (2013), Recent progress (2007–2012) in permafrost isotope geochemistry, *Permafrost Periglac. Process.*, *24*(2), 138–145, doi:10.1002/ppp.1768.

Lara, M. J., et al. (2015), Polygonal tundra geomorphological change in response to warming alters future CO_2 and CH_4 flux on the Barrow Peninsula, *Global Change Biol.*, *21*, 1634–1651, doi:10.1111/gcb.12757.

Lee, J., X. Feng, A. M. Faiia, E. S. Posmentier, J. W. Kirchner, R. Osterhuber, and S. Taylor (2010), Isotopic evolution of seasonal snowcover and its melt by isotopic exchange between liquid water and ice, *Chem. Geol.*, *270*, 126–134, doi:10.1016/j.chemgeo.2009.11.011.

Lipson, D. A., M. Jha, T. K. Raab, and W. C. Oechel (2010), Reduction of iron (III) and humic substances plays a major role in anaerobic respiration in an Arctic peat soil, *J. Geophys. Res.*, *115*, G00I06, doi:10.1029/2009JG001147.

Lipson, D. A., D. Zona, T. K. Raab, F. Bozzolo, M. Mauritz, and W. C. Oechel (2012), Water-table height and microtopography control biogeochemical cycling in an Arctic coastal tundra ecosystem, *Biogeosciences*, *9*(1), 577–591, doi:10.5194/bg-9-577-2012.

Lipson, D. A., T. K. Raab, D. Goria, and J. Zlamal (2013), The contribution of Fe(III) and humic acid reduction to ecosystem respiration in drained thaw lake basins of the Arctic Coastal Plain, *Global Biogeochem. Cycles*, *27*, 399–409, doi:10.1002/gbc.20038.

Lis, G., L. I. Wassenaar, and M. J. Hendry (2008), High-precision laser spectroscopy D/H and $^{18}O/^{16}O$ measurements of microliter natural water samples, *Anal. Chem.*, *80*, 287–293, doi:10.1021/ac701716q.

Lougheed, V. L., M. G. Butler, D. C. McEwen, and J. E. Hobbie (2011), Changes in tundra pond limnology: Re-sampling Alaskan ponds after 40 years, *Ambio*, *40*(6), 589–599, doi:10.1007/s13280-011-0165-1.

Louiseize, N. L., M. J. Lafrenière, and M. G. Hastings (2014), Stable isotopic evidence of enhanced export of microbially derived NO_3^- following active layer slope disturbance in the Canadian High Arctic, *Biogeochemistry*, *121*, 565–580, doi:10.1007/s10533-014-0023-x.

Mack, M. C., E. A. G. Schuur, M. S. Bret-Harte, G. R. Shaver, and F. S. Chapin (2004), Ecosystem carbon storage in arctic tundra reduced by long-term nutrient fertilization, *Nature*, *431*(7007), 440–443, doi:10.1038/nature02887.

Mackay, J. R. (1974), Ice-wedge cracks, Garry Island, Northwest Territories, *Can. J. Earth Sci.*, *11*(10), 1366–1383, doi:10.1139/e74-133.

Mackay, J. R. (1983), Downward water movement into frozen ground, western arctic coast Canada, *Can. J. Earth Sci.*, *20*(1), 120–134, doi:10.1139/e83-012.

Mackay, J. R. (2000), Thermally induced movements in ice-wedge polygons, western arctic coast: A long-term study, *Geogr. Phys. Quatern.*, *54*(1), 41–68, doi:10.7202/004846ar.

Meyer, H., et al. (2010), Lateglacial and Holocene isotopic and environmental history of northern coastal Alaska—Results from a buried ice-wedge system at Barrow, *Quaternary Sci. Rev.*, *29*(27–28), 3720–3725, doi:10.1016/j.quascirev.2010.08.005.

Michel, F. A. (1990), Isotopic composition of ice-wedge ice in northwestern Canada, Proceedings, Fifth Canadian Permafrost Conference, Nordicana 54, 5–9, doi:10.1016/j.quascirev.2010.08.005.

Morin, S., J. Savarino, M. M. Frey, N. Yan, S. Bekki, J. W. Bottenheim, and J. M. F. Martins (2008), Tracing the origin and fate of NOx in the Arctic atmosphere using stable isotopes in nitrate, *Science*, *322*(5902), 730–732, doi:10.1126/science.1161910.

Nadelhoffer, K. J., A. E. Giblin, G. R. Shaver, and J. A. Laundre (1991), Effects of temperature and substrate quality on element mineralization in six arctic soils, *Ecology*, *72*(1), 242–253, doi:10.2307/1938918.

Neff, J. C., A. R. Townsend, G. Gleixner, S. J. Lehman, J. Turnbull, and W. D. Bowman (2002), Variable effects of nitrogen additions on the stability and turnover of soil carbon, *Nature*, *419*(6910), 915–917, doi:10.1038/nature01136.

Newman, B. D., et al. (2015), Microtopographic and depth controls on active layer chemistry in Arctic polygonal ground, *Geophys. Res. Lett.*, *42*, 1808–1817, doi:10.1002/2014GL062804.

Nowak, A., and A. Hodson (2014), On the biogeochemical response of a glacierized High Arctic watershed to climate change: Revealing patterns, processes and heterogeneity among micro-catchments, *Hydrol. Process.*, doi:10.1002/hyp.10263, in press.

Nowinski, N. S., S. E. Trumbore, E. A. G. Schuur, M. C. Mack, and G. R. Shaver (2008), Nutrient addition prompts rapid destabilization of organic matter in an arctic tundra ecosystem, *Ecosystems*, *11*(1), 16–25, doi:10.1007/s10021-007-9104-1.

Raynolds, M. K., D. A. Walker, K. J. Ambrosius, J. Brown, K. R. Everett, M. Kanevskiy, G. P. Kofinas, V. E. Romanovsky, Y. Shur, and P. J. Webber (2014), Cumulative geoecological effects of 62 years of infrastructure and climate change in ice-rich permafrost landscapes, Prudhoe Bay Oilfield, Alaska, *Global Change Biol.*, *20*, 1211–1224, doi:10.1111/gcb.12500.

Rowland, J. C., et al. (2010), Arctic landscapes in transition: Responses to thawing permafrost, *Eos Trans. AGU*, *91*(26), 229–230, doi:10.1029/2010EO260001.

Roy Chowdhury, T., E. M. Herndon, T. J. Phelps, D. A. Elias, B. Gu, L. Liang, S. D. Wullschleger, and D. E. Graham (2015), Stoichiometry and temperature sensitivity of methanogenesis and CO_2 production from saturated polygonal tundra in Barrow, Alaska, *Global Change Biol.*, *21*, 722–737, doi:10.1111/gcb.12762.

Savarino, J., J. Kaiser, S. Morin, D. M. Sigman, and M. H. Thiemens (2007), Nitrogen and oxygen isotopic constraints on the origin of atmospheric nitrate in coastal Antarctica, *Atmos. Chem. Phys.*, *7*(8), 1925–1945.

Schuur, E. A. G., et al. (2008), Vulnerability of permafrost carbon to climate change: Implications for the global carbon cycle, *BioScience*, *58*(8), 701–714, doi:10.1641/b580807.

Seeberg-Elverfeldt, J., M. Schluter, T. Feseker, and M. Kolling (2005), Rhizon sampling of porewaters near the sediment-water interface of aquatic systems, *Limnol. Oceanogr.: Methods*, *3*, 361–371, doi:10.4319/lom.2005.3.361.

Shaver, G. R., W. D. Billings, F. S. Chapin, A. E. Giblin, K. J. Nadelhoffer, W. C. Oechel, and E. B. Rastetter (1992), Global change and the carbon balance of Arctic ecosystems, *BioScience*, *42*(6), 433–441, doi:10.2307/1311862.

Shiklomanov, N. I., D. A. Streletskiy, F. E. Nelson, R. D. Hollister, V. E. Romanovsky, C. E. Tweedie, J. G. Bockheim, and J. Brown (2010), Decadal variations of active-layer thickness in moisture-controlled landscapes, Barrow, Alaska, *J. Geophys. Res.*, *115*, G00I04, doi:10.1029/2009JG001248.

Sigman, D. M., K. L. Casciotti, M. Andreani, C. Barford, M. Galanter, and J. K. Bohlke (2001), A bacterial method for the nitrogen isotopic analysis of nitrate in seawater and freshwater, *Anal. Chem.*, *73*(17), 4145–4153, doi:10.1021/ac010088e.

Smith, L. C., Y. Sheng, G. M. MacDonald, and L. D. Hinzman (2005), Disappearing Arctic lakes, *Science*, *308*(5727), 1429–1429, doi:10.1126/science.1108142.

Sturm, M., J. Schimel, G. Michaelson, J. M. Welker, S. F. Oberbauer, G. E. Liston, J. Fahnestock, and V. E. Romanovsky (2005), Winter biological processes could help convert arctic tundra to shrubland, *BioScience*, *55*(1), 17–26, doi:10.1641/0006-3568(2005)055[0017:wbpchc]2.0.co;2.

Tye, A. M., and T. H. E. Heaton (2007), Chemical and isotopic characteristics of weathering and nitrogen release in non-glacial drainage waters on Arctic tundra, *Geochim. Cosmochim. Acta*, *71*(17), 4188–4205, doi:10.1016/j.gca.2007.06.040.

Vaikmäe, R. (1989), Oxygen isotopes in permafrost and ground ice—A new tool for paleoclimatic investigations, 5th Working Meeting Isotopes in Nature, Proceedings, pp. 543–553, Leipzig, Germany.

Walter, K. M., et al. (2014), A shift of thermokarst lakes from carbon sources to sinks during the Holocene epoch, *Nature*, *511*(7510), 452–456, doi:10.1038/nature13560.

Weintraub, M. N., and J. P. Schimel (2003), Interactions between carbon and nitrogen mineralization and soil organic matter chemistry in arctic tundra soils, *Ecosystems*, *6*(2), 129–143, doi:10.1007/s10021-002-0124-6.

Weintraub, M. N., and J. P. Schimel (2005), Nitrogen cycling and the spread of shrubs control changes in the carbon balance of Arctic Tundra ecosystems, *BioScience*, *55*(7), 551–551, doi:10.1641/0006-3568(2005)055[0408:NCATSO]2.0.CO;2.

Wynn, P. M., A. J. Hodson, T. H. E. Heaton, and S. R. Chenery (2007), Nitrate production beneath a High Arctic Glacier, Svalbard, *Chem. Geol.*, *244*(1–2), 88–102, doi:10.1016/j.chemgeo.2007.06.008.

Xu, C., C. Liang, S. Wullschleger, C. Wilson, and N. McDowell (2011), Importance of feedback loops between soil inorganic nitrogen and microbial communities in the heterotrophic soil respiration response to global warming, *Nat. Rev. Microbiol.*, *9*(3), 222, doi:10.1038/nrmicro2439-c1.

Xue, D., J. Botte, B. De Baets, F. Accoe, A. Nestler, P. Taylor, O. Van Cleemput, M. Berglund, and P. Boeckx (2009), Present limitations and future prospects of stable isotope methods for nitrate source identification in surface- and groundwater, *Water Res.*, *43*(5), 1159–1170, doi:10.1016/j.watres.2008.12.048.

Zona, D., D. A. Lipson, R. C. Zulueta, S. F. Oberbauer, and W. C. Oechel (2011), Microtopographic controls on ecosystem functioning in the Arctic Coastal Plain, *J. Geophys. Res.*, *116*, G00I08, doi:10.1029/2009JG001241.